Journal of Zhejiang University-SCIENCE A (Applied Physics & Engineering)
ISSN 1673-565X (Print); ISSN 1862-1775 (Online)
www.jzus.zju.edu.cn; link.springer.com
E-mail: jzus_a@zju.edu.cn

A study of water curtain parameters of underground oil storage caverns using time series monitoring and numerical simulation*

Yi-guo XUE†, Ze-xu NING, Dao-hong QIU, Mao-xin SU, Zhi-qiang LI,
Fan-meng KONG, Guang-kun LI, Peng WANG

Research Center of Geotechnical and Structural Engineering, Shandong University, Jinan 250061, China

†E-mail: xieagle@sdu.edu.cn

Received Mar. 31, 2020; Revision accepted July 7, 2020; Crosschecked Feb. 20, 2021

Abstract: Water curtain systems (WCSs) are key components for the operation of underground oil storage caverns (UOSCs) and their optimization and design are important areas of research. Based on the time series monitoring of the first large-scale underground water-sealed storage cavern project in China, and on finite element analysis, this study explores the optimum design criteria for WCSs in water-sealed oil caverns. It shows that the optimal hole spacing of the WCS for this underground storage cavern is 10 m in order to ensure seal effectiveness. When the WCS is designed with a 10-m horizontal hole spacing and a water curtain pressure (WCP) of 80 kPa, a water curtain hole (WCH) has an influence radius of approximately 25 m. The smaller the vertical distance is between a WCH and the main cavern, the greater the water inflow into the main cavern. The vertical hydraulic gradient criterion can be satisfied when this distance is 25 m. It shows that the optimal WCP is 70 kPa, which meets sealing requirements.

Key words: Underground oil storage; Water curtain system (WCS); Water-sealed cavern; Optimum design criteria; Monitoring data; Finite element method (FEM)
https://doi.org/10.1631/jzus.A2000130 **CLC number:** TU91

1 Introduction

Underground oil storage caverns (UOSCs) are widely used due to their considerable safety benefits, limited land use, low pollution, low construction capital investment requirements, and low operation and maintenance costs compared with traditional underground oil depots (Ma et al., 2017). In the 1930s, the Swedish government transferred its oil reserves from surface storage to underground caverns, and with this started the exploration of the use of UOSCs. In 1949, a 30 m^3 test bank was created in Stockholm to store 17.6 m^3 of gasoline. The quality and volume of gasoline did not change during the test period, which proved the feasibility of using UOSCs. Typically, the geological parameters of areas selected for UOSCs are obtained using triaxial testing and in situ horizontal stress tests. Based on a multiphase, multicomponent approach, a cavern thermodynamic model that can be used in field applications has been created for this purpose (Rouabhi et al., 2017). Table 1 provides a summary of some UOSC projects, focusing on the comparison of parameters for water curtain holes (WCHs) in underground caverns with horizontal WCHs (Lee and Song, 2003; Levinson et al., 2004). As shown, the size and design parameters of the Korean U-2 and Chinese Huangdao oil caverns are similar, making the U-2 cavern an effective reference for the Huangdao cavern.

* Project supported by the National Natural Science Foundation of China (Nos. 41877239, 51379112, 51422904, 40902084, and 41772298), the Fundamental Research Funds for the Central Universities (No. 2018JC044), and the Natural Science Foundation of Shandong Province (No. JQ201513), China
ORCID: Yi-guo XUE, https://orcid.org/0000-0001-9928-5947

A hyperbolic shear strength criterion has been proposed based on a large amount of experimental data, which can be applied to predict the peak shear strength of rock joints in a range of samples tested in the laboratory (Tang et al., 2016). Point load tests and Schmidt hammer tests can be used to estimate uniaxial compressive rock strength (Kong and Shang, 2018; Shang et al., 2018). Relevant parameters of rock blocks and joints needed for calculation can also be obtained through rock triaxial compression tests and shear-seepage coupling tests of geological discontinuities (Li Y et al., 2017; Ma et al., 2017; Wu et al., 2019). Rock fractures separate intact rock blocks with negligible matrix permeability, and a fractal model has been established to assess the equivalent permeability of 2D rock fracture networks (Liu et al., 2015). The genetic programming (GP) method can be used to predict steady water inflow and the volume flow rate provided by the WCH, and the water inflow sensitivity to various WCH parameters is studied using regression analysis (Ravandi et al., 2018). A 3D simulation of the seepage field for a UOSC shows that the three factors essential for improving water-seal effects are: safety index, hydraulic gradient, and flow rate (Li Y et al., 2017; Ehlers, 2018).

The water sealing and deformation characteristics of UOSC are evaluated based on the fluid-solid coupling theory of discrete media (Chen et al., 2012; Li SC et al., 2012; Cornet, 2016; Li Y et al., 2017). However, the performance of the water curtain system (WCS) depends on the design of key parameters, and the influence of WCS with different parameters on the water sealing and stability of caverns varies. Data monitoring can be used to study patterns of large-scale change in a project. Typically, construction data are analyzed using time series analysis (autocorrelation and cross-correlation models) to assess the functional efficiency of WCSs in heavy rainfall areas (Yan et al., 2017; Shi et al., 2018).

Most of the above studies are focused on the stability, water sealing, and mechanical properties of UOSCs. However, little research has been done on WCSs in low-precipitation areas, and the influence of key parameters on the effectiveness of the WCSs has yet to be described. The UOSC sizes, stored mediums, and rock types are also different for different functions. To a certain extent, the design of WCSs for UOSCs in China lacks corresponding theoretical support. Together with the geologic exploration report and monitoring data from the Huangdao UOSC, this paper discusses the design criteria of WCSs by using the finite element method (FEM), and three parameters are analyzed and designed. The results can provide an important basis for the design of WCSs for underground water-sealed oil caverns in China.

2 Study area

2.1 Geology and hydrogeology

The Huangdao UOSC is a project located in Huangdao District, Qingdao, China. The Huangdao UOSC project comprises primarily nine main caverns, two construction tunnels, three connecting tunnels, and five water curtain tunnels. The main cavern is designed to be 20 m wide and 30 m high, with a straight wall and circular arch. The distance between the main cavern and the adjacent cavern is 30 m, and that between the connecting tunnel and the adjacent cavern is 25 m (Li et al., 2014). The designed storage pressure of the Huangdao UOSC is 100 kPa. The dip angles of the geological discontinuities are given in

Table 1 Parameters of some UOSC projects

UOSC project	Stored item	Volume ($\times10^4$ m^3)	Rock type	Key parameters for WCS			
				Hole spacing (m)	Hole length (m)	Vertical distance (m)	Orientation
Pyongtaek*, Korea	LPG	22.4	Gneiss	10	100–120	25	Horizontal, vertical
K-1, Korea	Gasoline	23	Granite	12	100–120	15	Horizontal
U-2, Korea	Crude oil	429.3	Diorite	7, 14	110	20	Horizontal
Ningbo, China	LPG	50	Tuff	10	100	10	Horizontal
Huangdao, China	Crude oil	300	Gneiss	10	97–110	25	Horizontal

* This is an extension project. LPG represents liquefied petroleum gas

Table 2. They show that more than half of the geological discontinuities near the main caverns are steep. In Fig. 1a, a group of 135°∠66° surface faults are strongly developed, indicated by a solid line. Figs. 1b and 1c show the engineering geology of the main caverns. The dashed lines indicate the dip angles of geological discontinuities.

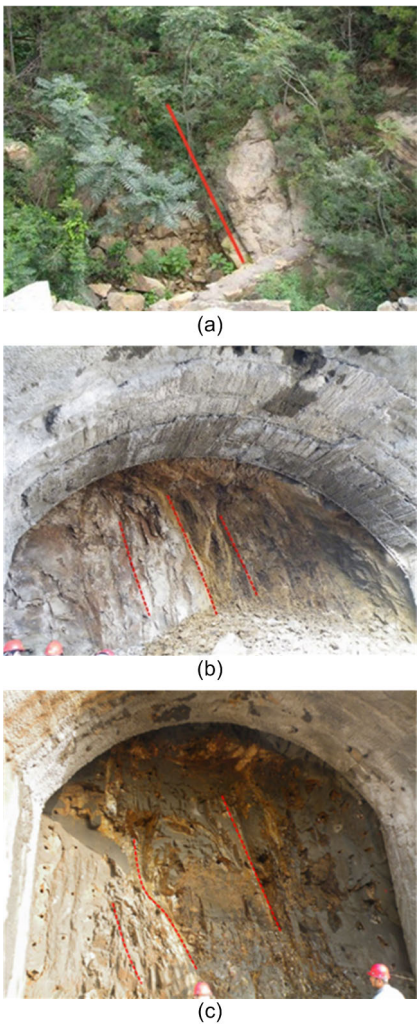

Fig. 1 Location of surface fault and tunnel faces of main caverns: (a) schematic of surface fault; (b) tunnel face 0+430 of the No. 1 main cavern; (c) tunnel face 0+137 of the No. 3 main cavern

Engineering geology and hydrogeological conditions are critical to the design of WCSs for water-sealed storage caverns. Based on an investigation of the engineering geology, the main lithology in the study area is pale red to light green-gray granitic gneiss, and the main minerals are quartz, plagioclase, and hornblende (Li et al., 2020). Table 3 gives the proportion of each rock mass classification present within the study area (Li et al., 2019). Most of the surrounding rocks are class II and class III, and the overall stability is good. Atmospheric precipitation is the main supplementary source of groundwater. Annual average precipitation ranges from 711.2 mm to 798.6 mm, and the average precipitation infiltration replenishment is 53.8 mm. This survey report specifies the horizontal plane 20 m above the cavern vault as the zero base level. In the course of this study, water levels of wells and surface water around the study area were observed and measured; the water level depth was 0.00–10.77 m. Water level elevation, which was basically consistent with the topography, ranged from 39.00 m to 125.35 m.

Table 2 Dip angles of the geological discontinuities near the main caverns

Dip (°)	Percentage (%)	Dip (°)	Percentage (%)
0–20	1	50–60	10
20–30	3	60–70	21
30–40	6	70–80	21
40–50	14	80–90	24

Table 3 Proportion of each rock mass classification in the surrounding rocks of caverns

Rock mass classification	Percentage (%)
I	8
II	56
III	21
IV	8
V	7

2.2 Geomechanical properties

The in-situ geometrical apertures of joints were measured on the sidewall of caverns after excavation using a stainless steel feeler gauge. A total of nine hydraulic transmissible joints in different places were measured; to obtain joint roughness coefficients (JRCs), fresh joint surfaces were mapped using a simple profiler. Mechanical properties were obtained using direct shear tests, and rock joints were prepared via Brazilian splitting of intact rock specimen (Li et al., 2014; Shang et al., 2016).

Fracture width and spacing ranges were obtained using extensive sampling and statistics. Core boring

on site as well as in-room cutting and polishing meant that processing size was 54 mm in diameter and 100 mm in height. Indoor triaxial tests were carried out on specimens using a rock rheometer RLW-1000 (Fig. 2). Confining pressures were set at 3 MPa, 6 MPa, and 10 MPa, respectively, while rock mechanical parameters such as cohesion, saturated uniaxial compressive strength, internal friction angle, and elastic modulus were obtained (Li et al., 2012; Shang et al., 2017; Aliyu et al., 2019). Poisson's ratio was calculated by measuring longitudinal and shear wave speeds. Results are summarized in Table 4.

Fig. 2 Triaxial rock rheometer RLW-1000

3 Underground water-sealed oil storage technology

3.1 Principle of water-sealed oil storage

The efficacy of WCSs has been well documented (Li et al., 2014). When the groundwater is unstable, a WCS is the best way to ensure effective water-seal performance. Water sealing is a core technology used in the construction and operation of UOSCs and must meet stringent requirements of stability. The water-seal condition and the rock mass strength are the primary controlling factors in site selection (Li ZQ et al., 2017). UOSCs should be built in rock mass at a certain depth below the stable groundwater level with good stability. In practical engineering, we can utilize a natural water seal, an artificial water seal, or a combination of the two methods. However, the stable groundwater level in the studied project area is relatively low and groundwater is scarce, and thus, artificial water curtain sealing was chosen.

Table 4 Geomechanical parameters of surrounding rock and geological discontinuities

Parameter	Description
Category	Granitic gneiss below +20 m
Density (g/cm^3)	2.63
Saturated uniaxial compressive strength (MPa)	90.74
Softening coefficient	0.89
Elastic modulus (GPa)	52.7
Poisson's ratio	0.19
Fracture width (mm)	0.5–1.0
Fracture spacing (m)	0.64–1.60
Shear strength index	
Cohesion (MPa)	10.17
Internal friction angle (°)	71.14
Average geometrical aperture of the joints (mm)	
High inclination angle	0.02
Low inclination angle	0.01
JRC of the joints	
High inclination angle	5
Low inclination angle	8

The storage function of the UOSC is based on three basic conditions: (1) the specific gravity of oil is lower than that of water; (2) oil is insoluble in water and does not react with water; (3) the pore pressure around the cavern is greater than the oil pressure inside the cavern, resulting in an inward pressure gradient (Wang et al., 2015). When underground water penetrates into the cavern, this indicates that the medium storage pressure in the cavern is less than the underground water pressure around the cavern. Fig. 3 is an operation schematic of a typical UOSC (Xue et al., 2015).

3.2 Basis for determining water-seal validity

The main approaches for determining water seal validity states that if the vertical hydraulic gradient I_0 is greater than 1, the cavern is sealed (Åberg, 1978). It is believed that as long as the pressure of all possible leakage passages is increased, leakage will not occur. As shown in Fig. 4, the water pressure on the left side of the chart is greater than the gravity stress, and the vertical hydraulic gradient is greater than 1, satisfying sealing requirements.

3.3 Arrangement of WCHs

In practical engineering, several methods are typically used to arrange WCHs: horizontal

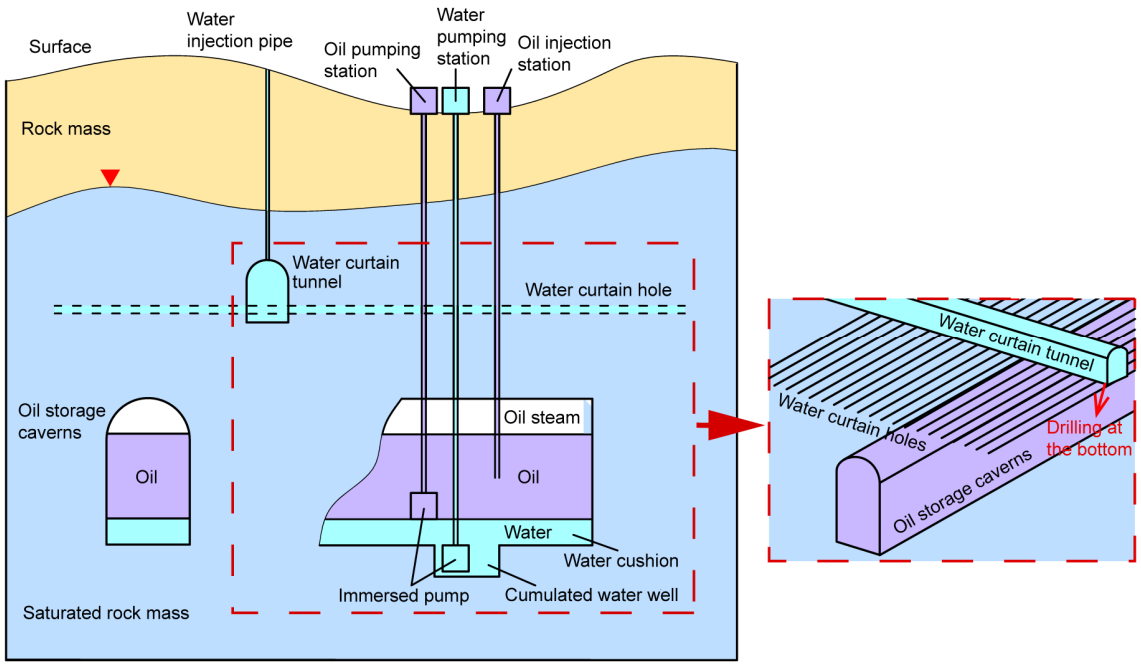

Fig. 3 Operation schematic of a typical UOSC

arrangements, vertical arrangements, and inclined arrangements. The arrangement of WCHs should satisfy several conditions: (1) the direction of a WCH is perpendicular to the main direction of seepage; (2) the WCH connects geological discontinuities to the greatest possible extent, that is, in a direction perpendicular to geological discontinuities to ensure maximum effectiveness (Li et al., 2014; Xu et al., 2018). In consideration of the engineering geological conditions of this region, with relatively steeply dipping geological discontinuities, a horizontal hole arrangement was adopted in this project to maximize the connections between the WCHs and geological discontinuities (Fig. 5).

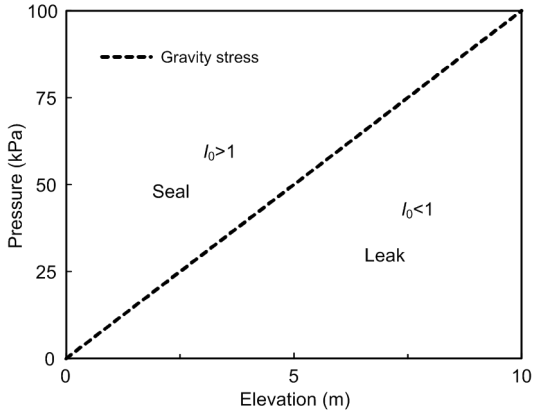

Fig. 4 Indication of the water seal criterion

4 Time series monitoring and analysis during the operation period

Monitoring is the best method to observe and evaluate the operational effect of a UOSC, and monitoring data can best reflect the characteristics of the underground coupling field. A time series analysis is suitable for a long-time data series containing seasonality, and studying its regularity helps us understand the mechanisms of storage and propose optimization measures. According to specifications, the

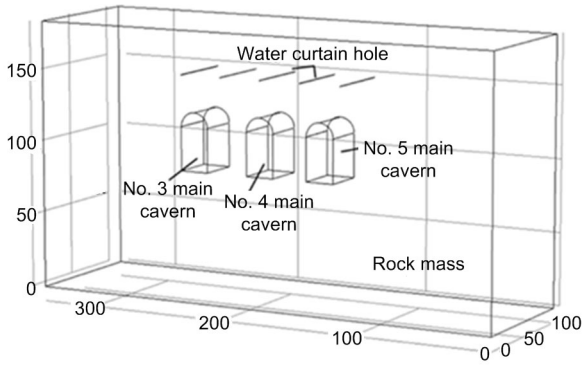

Fig. 5 Arrangement of caverns and horizontal WCH (unit: m)

UOSC will be permanently monitored once production begins.

4.1 Seepage pressure monitoring

A vibrating wire osmometer was used to monitor seepage pressure in the water curtain tunnels. Before operation, monitoring holes were drilled and five to six osmometers were buried at different elevations, that is, layered and sectional osmometers were buried. Fig. 6 shows the location of monitoring points used in the study and Table 5 shows the seepage pressure of measurement points PA1 from Jan. 1, 2018 to May 1, 2018. According to the series data, because of the different elevation, the seepage pressure is different, and the range of change with time is also different.

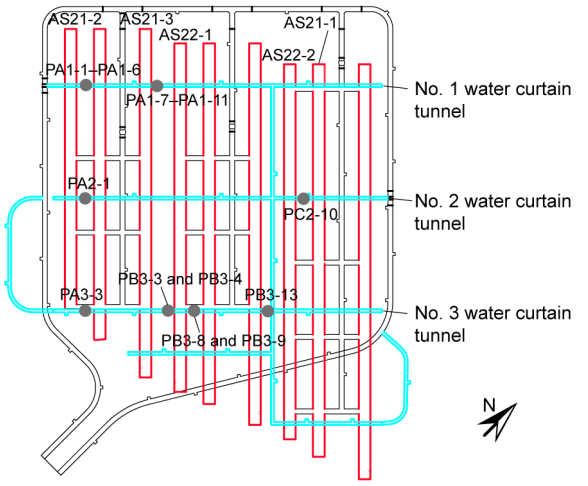

Fig. 6 Location of monitoring points

AS: oil-gas pressure monitoring points; PA, PB, and PC: seepage pressure monitoring points

Table 5 Time series seepage pressure of group PA1 from Jan. 1, 2018 to May 1, 2018

Serial number	Seepage pressure (kPa)				
	Jan. 1	Feb. 1	Mar. 1	Apr. 1	May 1
PA1-1	217.55	217.72	217.10	216.32	215.79
PA1-2	102.57	102.47	102.38	101.40	100.92
PA1-3	7.18	7.85	8.72	9.51	10.18
PA1-4	5.53	6.01	6.58	6.87	7.25
PA1-5	166.44	164.23	160.65	154.77	148.01
PA1-6	344.20	327.77	338.72	342.05	347.90
PA1-7	232.94	232.66	232.38	231.45	230.72
PA1-8	110.80	110.41	110.51	110.22	109.83
PA1-9	155.18	154.34	153.15	153.05	151.93
PA1-10	258.88	254.86	255.35	253.69	251.38
PA1-11	323.49	314.87	316.72	314.24	310.53

The seepage pressure at each monitoring point conforms to the vertical hydraulic gradient criterion at the corresponding elevation, indicating that the water-sealing can meet requirements. However, in many places the seepage pressure is large, resulting in excessive water flow. Because of the WCS, the seepage pressure no longer conforms to $p=\rho gh$ (where p is the pore pressure, ρ is the density of water, g is the acceleration of gravity, and h is the depth below the water level). The overall seepage pressure shows a decreasing trend, indicating that the seepage pressure should be replenished through the WCS.

When considering the time effect, some representative monitoring points were selected to analyze the long-term monitoring data of seepage pressure around the cavern. Fig. 7 shows the seepage pressures of the monitoring points in 2018, in which the seepage pressure data of PA1-6 on Mar. 1 was not measured due to equipment damage.

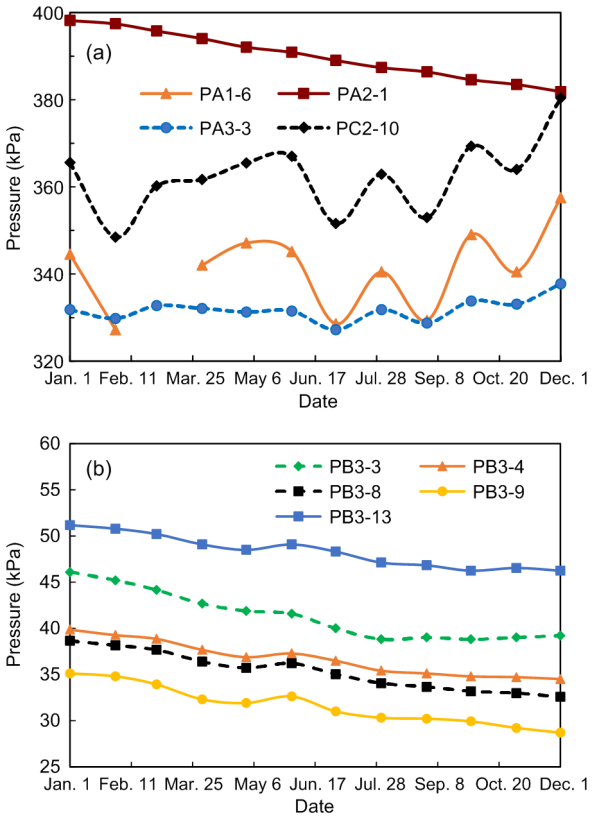

Fig. 7 Seepage pressures of the monitoring points

(a) PA and PC; (b) PB

As can be seen from Fig. 7, the seepage pressure at the point PA1-6 fluctuated greatly, with a minimum

value of 327.2 kPa and a maximum value of 357.49 kPa. Consistent with the trend of change at PA1-6, the difference in seepage pressure at PC2-10 within one year was 31.96 kPa. The monitoring point of PA2-1 showed a decline, with a cumulative decline of 16.34 kPa from Jan. 1 to Dec. 1. The range of change of PA3-3 was small, and the pressure was largely stable. PB3-3, PB3-4, PB3-8, PB3-9, and PB3-13 all showed the same downward and fluctuating trends.

Seepage pressure should be maintained regularly. The seepage pressure monitoring analysis of the UOSC during the operation period shows that the WCS design used during construction is not fully effective. In other words, the economic benefits and functions of the water curtain are not maximized and thus the WCS needs to be further optimized.

4.2 Oil-gas pressure monitoring

In addition to oil and water inside the cavern, there is a small amount of oil-gas. Water inflow cannot be measured directly, but it can be seen indirectly by monitoring the oil-gas pressure. When there is too much water in the cavern, the oil-gas pressure increases and is detected by a barometer buried in the cavern. The water in the cavern is then pumped out to reduce the pressure. The oil-gas pressure monitoring points corresponding to the caverns studied are shown at the top of Fig. 6.

Fig. 8 compares the characteristics of five pressure series. The values for the five groups show the same obvious seasonality. In April and May, the pressure was higher, and surface rainfall caused a larger water inflow into the cavern. The pressure was the lowest in November. Special attention should be paid to cavern No. 4 corresponding to AS22-1, which has long been under negative pressure and in which negative pressure has increased significantly, from −33.15 MPa to −64.09 MPa. The negative pressure environment indicates that oil steam may leak along a fracture passage at the vault. This may be due to low seepage pressure around the cavern. It did not meet the third storage function condition, i.e. an inward pressure gradient. This illustrates that the water curtain pressure (WCP) should not be too large (an increased water inflow), nor too small (oil leakage). The parameters of the water curtain need further optimization.

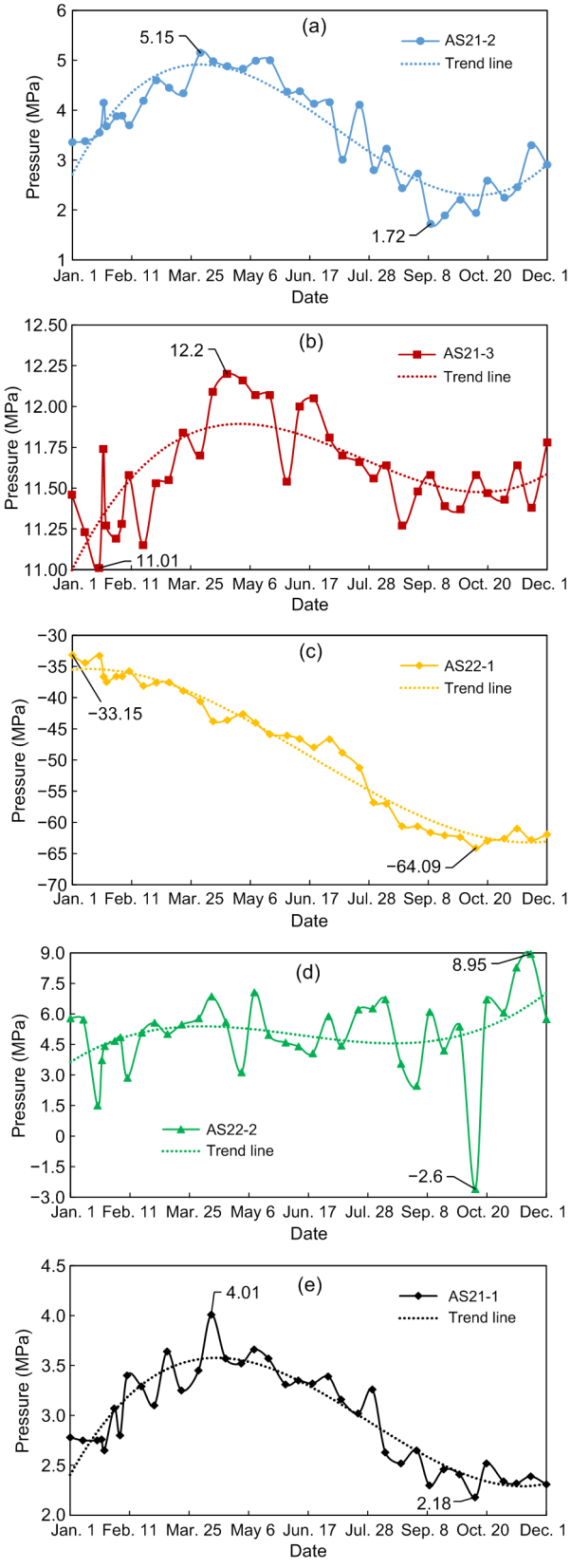

Fig. 8 Oil-gas pressures of the monitoring points: (a) AS21-2; (b) AS21-3; (c) AS22-1; (d) AS22-2; (e) AS21-1

5 Optimum design of the water curtain parameters

Research on UOSCs involves the combination of multiple physical fields, such as stress and seepage (Yang et al., 2014; Ye et al., 2019). This type of problem can be addressed using Darcy's law, proposed by French hydrologist Henry Darcy in 1856, which concerns the seepage of underground water in porous media such as rock and soil. Using the FEM, a complex model is simplified to many continuous subdomains, and then the approximate solution of the problem is obtained.

Assuming that the seepage of the caverns obeys Darcy's law, his formula, expressed by pore pressure, is as follows:

$$v=-\frac{1}{\gamma_{\mathrm{w}}}k\frac{\partial(p+\gamma_{\mathrm{w}}z)}{\partial x}, \tag{1}$$

where k is the medium permeability coefficient; γ_{w} is the water unit weight; v is the seepage velocity of groundwater; z is the vertical coordinate; x is the distance along the X axis.

Boundary and initial conditions must be considered when addressing seepage problems in rock strata. The distribution of the water head can be determined by solving differential equations. According to the principle of effective stress in porous media, the basic equation for a seepage field is as follows:

$$S\frac{\partial p}{\partial t}+\nabla\cdot\left[-\frac{k}{\gamma_{\mathrm{w}}}\nabla(p+\gamma_{\mathrm{w}}z)\right]=Q-\eta\frac{\partial}{\partial t}(\nabla\cdot\boldsymbol{\mu}), \tag{2}$$

where S is the medium storage coefficient; t is the time; Q is the volume source; η is the rock porosity; $\boldsymbol{\mu}$ is the velocity vector of underground water.

It is obvious that the seepage equation is nonlinear, but it can be regarded as linear in a microsegment of pore pressure change:

$$q_i=-(k\varphi)_{ti}, \tag{3}$$

where q_i is the velocity component of water seepage; φ is the pressure potential. Since the density of water is 1 g/cm^3, there is

$$\varphi=\frac{p}{g}, \tag{4}$$

thus,

$$q_i=-\left(k\frac{p}{g}\right)_{ti}, \tag{5}$$

where the permeability coefficient of rock mass is nonlinear and the relationship between porosity and the permeability coefficient is satisfied:

$$k=k_0\left(\frac{\eta}{\eta_0}\right)^3, \tag{6}$$

where k_0 is the initial permeability coefficient and η_0 is the initial porosity (Kjørholt and Broch, 1992). In engineering calculations, the fixed permeability coefficient is used instead of the nonlinear value to simplify the calculation process:

$$k=a_0\cdot\exp(-a_1\Theta), \tag{7}$$

where Θ is effective volume stress; a_0 and a_1 are testing constants.

The water content in saturated rock is the sum of adsorbed water W_{C} and free water W_{CB}, where

$$W_{\mathrm{C}}=\frac{abp}{1+bp}r_{\mathrm{m}}\rho, \tag{8}$$

$$W_{\mathrm{CB}}=\eta\frac{p}{p_0}\rho, \tag{9}$$

and thus the water content is

$$W=W_{\mathrm{C}}+W_{\mathrm{CB}}=\left(\frac{abp}{1+bp}r_{\mathrm{m}}+\eta\frac{p}{p_0}\right)\rho, \tag{10}$$

where W_{C} is the amount of adsorbed water in rock mass per unit volume; a is the maximum water adsorption in rock mass; b is the adsorption constant of rock mass; r_{m} is the weight of rock mass; W_{CB} is the amount of free water in rock mass per unit volume; p_0 is standard air pressure.

When establishing a coordinate system at the predominant seepage axis, the seepage equation in saturated rock mass is

$$\frac{\partial}{\partial x}\left(k_x\frac{\partial p}{\partial x}\right)+\frac{\partial}{\partial y}\left(k_y\frac{\partial p}{\partial y}\right)+\frac{\partial}{\partial z}\left(k_z\frac{\partial p}{\partial z}\right)=\left[\frac{2\eta}{p_0}+\frac{abr_{\mathrm{m}}}{(1+bp)^2}+\frac{abr_{\mathrm{m}}}{1+bp}\right]\frac{\partial p}{\partial t}. \tag{11}$$

Water-sealed oil storage is affected by the coupling of underground media including solids, liquids, gases, and geological discontinuities such as faults. The calculation model adopted in this study is the equivalent continuum model. It is assumed that the minimum material substance constituting a fluid is the fluid particle, which is regarded as continuous. In numerical simulations, the 3D problem is simplified as a plane strain problem (Hou and Shu, 2016). To study WCH spacing and the vertical distance between the WCHs and main cavern, the Nos. 3–5 caverns were used as simulation objects. These two sections focus mainly on the distribution of seepage pressure in the upper part of the No. 4 cavern. Additionally, the influences of adjacent caverns (i.e. No. 3 and No. 5 caverns) were considered. When studying the WCP, it is necessary to consider the topography. The topographic conditions and initial pore pressure of the nine main caverns must be considered simultaneously.

5.1 WCH spacing

The model applied here simplifies complex terrain into a rectangular region, 340 m in length, 100 m in width, and 180 m in height. The cavern used for this analysis is 20 m wide and 30 m high and has an arched top, while the distance between the left and right sides as well as the middle cavern are 30 m and 20 m, respectively. A horizontal range of 25 m above the top of the main cavern was arranged with WCHs; these have a diameter of 120 mm and are arranged above caverns in the same direction as these features. Table 6 presents medium parameters used in this simulation. Thus, throughout the modeling process, a series of hypotheses were applied including that, in the first place, rock mass is considered a homogeneous, isotropic equivalent continuum. Secondly, the deformation of rock mass and caverns conforms to an elastic-plastic hydrodynamic model but is not encompassed in this analysis. Thirdly, groundwater flow conforms to Darcy's law. Fourthly, the initial stress of a rock mass only considers gravity stress and so structural stress is not considered. In terms of constructing saturated granitic gneiss material, we set density, porosity, and permeability of the calculation area and then assumed the area of this to be a saturated porous medium. Thus, given the action of gravity, groundwater flows along pores so that pore pressure is calculated. The initial pore pressure distribution of the model is $p=\rho gh$. The boundary conditions of the fluid phase are as follows: the left and right sides are zero-flow boundaries, and the upper and lower boundaries are pressure boundaries that allow underground water to freely cross the boundary surface. During the operation period, the oil pressure distribution of the main cavern filled with oil is according to $p_{\mathrm{o}}=\rho_{\mathrm{o}}gh$, where p_{o} is the oil pressure, and ρ_{o} is the density of the oil. The oil-gas pressure at the cavern top was 0.1 MPa, the diameter of the WCHs was 120 mm, and the WCP was temporarily set to 80 kPa. According to current specifications, the vertical distance between the bottom of the water curtain tunnel and the top of a cavern should be no less than 20 m. Therefore, a vertical hydraulic gradient at 20 m above the top should be considered to ensure the effectiveness of the water curtain.

Table 6 Medium parameters used in the simulation

Parameter	Value
Rock density (g/cm^3)	2.63
Porosity	0.05
Permeability coefficient (m/d)	1×10^{-4}
Permeability (m^2)	1×10^{-15}
Oil density (kg/m^3)	850
Oil dynamic viscosity (Pa·s)	2×10^{-5}
Water density (kg/m^3)	1000
Water dynamic viscosity (Pa·s)	1.01×10^{-3}

Fig. 9 shows the pore pressure distributions and the fluid velocity vector distributions perpendicular to the axis direction of the main cavern at different spacings. This figure shows that the larger the WCH spacing is, the smaller the range of pressure influence, but the overall pressure distribution remains approximately the same. The arrows show the fluid velocity vector distribution, indicating the water-seal effect around the cavern under each WCH spacing. The fluid velocity near the main cavern is directed toward the cavern, indicating that water flows into the cavern, thus preventing oil leakage.

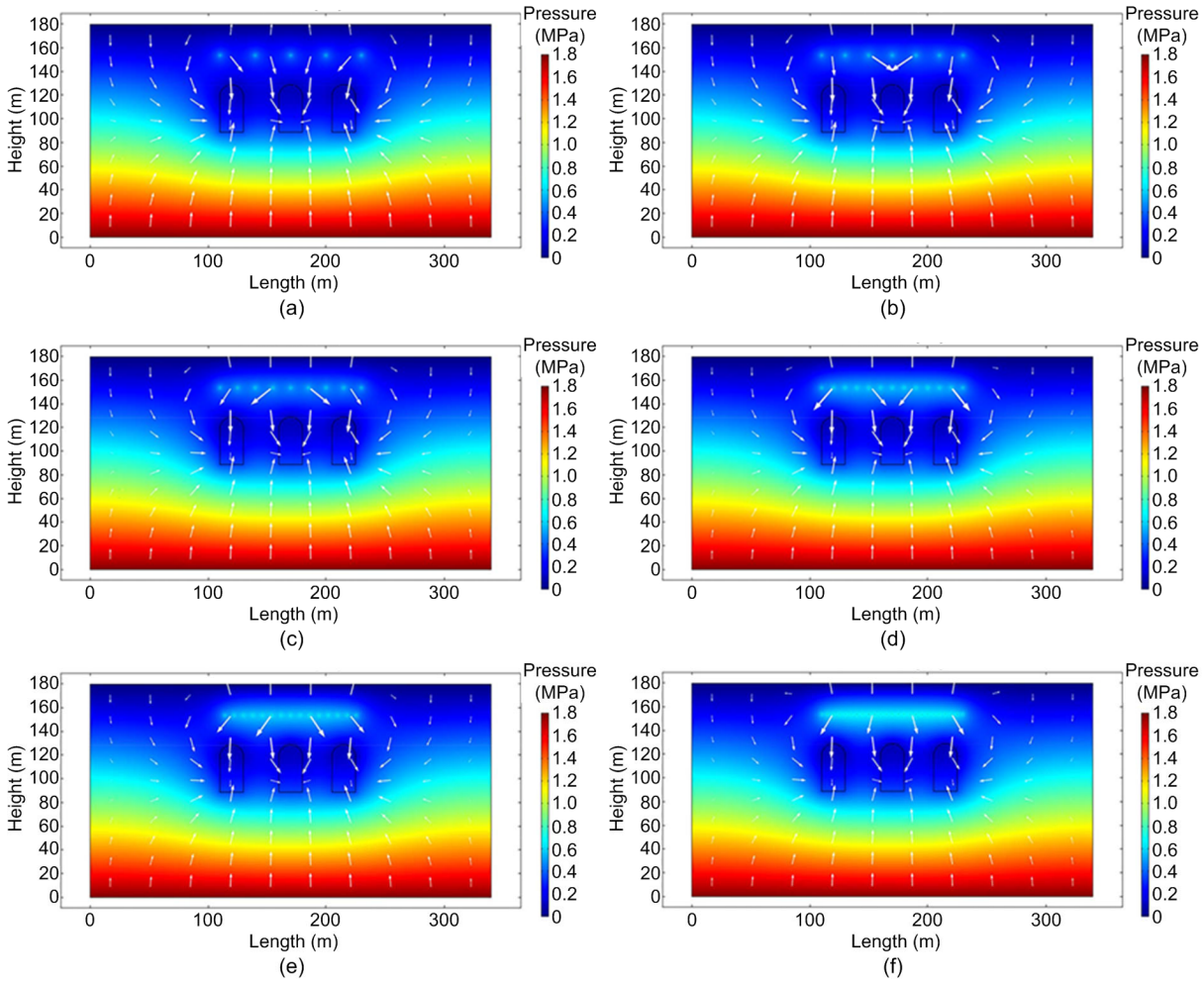

Fig. 9 Pore pressure distributions and fluid velocity vector distributions at different WCH spacings: (a) 30 m; (b) 20 m; (c) 15 m; (d) 10 m; (e) 8 m; (f) 5 m

The pore pressure acting perpendicular to the main cavern at an elevation of 0–25 m (Fig. 10) is used to create Fig. 11. Table 7 gives specific values of the pore pressures from Fig. 11. When the WCH spacing was greater than 10 m, the pressure clearly increased with decreased spacing. When the WCH spacing was less than 10 m, the pore pressure increased slowly and tended to be stable.

The pressures at elevation of 20 m were 0.58 MPa, 0.52 MPa, 0.49 MPa, 0.42 MPa, 0.38 MPa, and 0.33 MPa in the simulation (for tested WCH spacings of 5–30 m, respectively). Based on the geological survey, the gravity stress of the rock at an elevation of 20 m is estimated to be approximately 0.46 MPa. According to the vertical hydraulic gradient criterion, when the WCH spacing is 15–30 m, the pore pressure is less than the gravity stress and water sealing

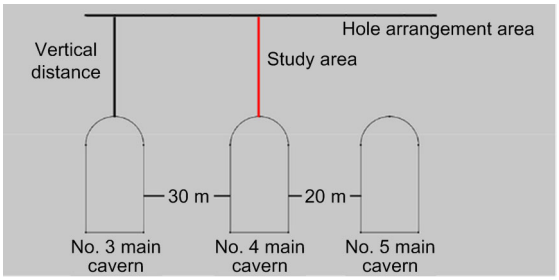

Fig. 10 Study area for Fig. 11

cannot be guaranteed. A WCS is designed to increase the water supply artificially to ensure that the cavern has sufficient water inflow, preventing the oil from leaking (Xu et al., 2018). However, excessive water inflow will reduce oil storage efficiency and increase drainage costs. In consideration of costs, 10 m was chosen as the optimum WCH spacing.

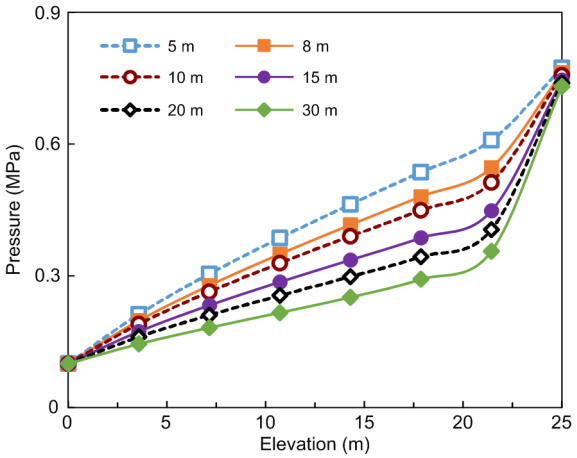

Fig. 11 Pore pressures at the elevation of 0–25 m at different WCH spacings (the horizontal plane at the top of the caverns is taken as the zero datum)

Table 7 Specific values of the pore pressures in Fig. 11

Elevation (m)	Pore pressure (MPa)					
	5 m	8 m	10 m	15 m	20 m	30 m
0.0	0.10	0.10	0.10	0.10	0.10	0.10
3.6	0.21	0.20	0.19	0.17	0.16	0.15
7.1	0.30	0.28	0.26	0.23	0.21	0.18
10.7	0.39	0.35	0.33	0.29	0.26	0.22
14.3	0.46	0.42	0.39	0.34	0.30	0.25
17.9	0.54	0.48	0.45	0.39	0.34	0.29
21.4	0.61	0.55	0.51	0.45	0.41	0.36
25.0	0.77	0.76	0.76	0.75	0.74	0.73

5.2 Vertical distance

Analysis was aimed at determining a reasonable vertical distance between the WCHs and the main cavern in the operation period. The WCHs were placed 20 m, 25 m, 30 m, or 35 m above the caverns. The WCH spacing was 10 m, the number of holes was 13, and the WCP was 80 kPa. Fig. 12 shows the pore pressure distributions and the fluid velocity vector distributions perpendicular to the axis of the main cavern for different vertical distances tested. The pore pressure distributions of the four simulations were generally consistent.

To explore the optimum vertical distance between WCHs and the main cavern, the pore pressure perpendicular to the main cavern at an elevation of 0–35 m (Fig. 10) was used to create Fig. 13. Table 8 shows the specific values of pore pressures shown in Fig. 13. With an increase in vertical distance, the pore pressure acting perpendicular to the cavern axis from 0 m to 35 m above the WCH increased correspondingly, and its distribution was regular. Within 5 m below the WCH, the slope of the break line increased, which indicates an obvious increase in pore pressure.

The pressures at an elevation of 20 m were 0.76 MPa, 0.49 MPa, 0.42 MPa, and 0.36 MPa in the simulation (for tested vertical distances of 20–35 m,

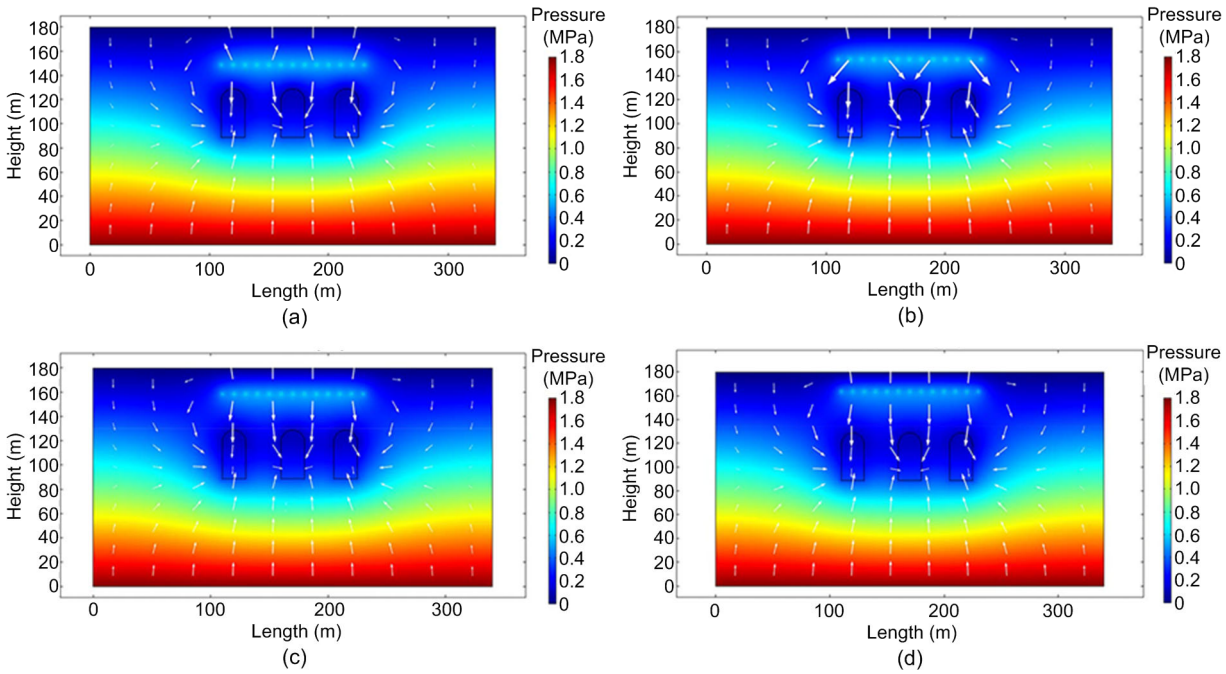

Fig. 12 Pore pressure distributions and fluid velocity vector distributions for different vertical distances between the WCHs and the main cavern: (a) 20 m; (b) 25 m; (c) 30 m; (d) 35 m

respectively), and the gravity stress of the rock was 0.46 MPa. According to the criterion of the vertical hydraulic gradient, when the vertical distance is 35 m to 30 m, water sealing cannot be guaranteed. When the WCH spacing is 10 m and the WCP is 80 kPa, the WCS has a vertical action range of approximately 25 m. To reduce water inflow, 25 m was chosen as the most reasonable vertical distance between WCHs and the main cavern.

5.3 WCP

In this section, the optimum WCP during the operation period is analyzed. The model body width was much longer than the width of a single cavern, and so the 3D problem was again simplified to a plane strain problem. The 2D model was reconstructed due to the influence of terrain factors. Nine caverns were arranged from west to east. The study scope is a 600-m extension of the left and right caverns (i.e. No. 1 and No. 9 caverns) to ensure that the boundary effects are sufficiently accounted for. Additionally, the rock mass extends up to the surface and down to 400 m from the cavern floor. The spacing between caverns reflects the actual spacing. The WCH spacing is 10 m, the vertical distance between the WCH and caverns is 25 m, and the number of holes is 55. The solid phase boundary conditions are as follows: the horizontal displacements of the left and right model sides are zero, the upper surface is a free displacement boundary, the lateral and longitudinal displacements of the lower boundary are zero, and the cavern wall has a zero-displacement boundary condition following excavation. The fluid phase boundary conditions are as follows: the left and right sides are zero-flow boundaries, and the upper and lower boundaries are pressure boundaries, allowing groundwater to flow freely across the boundary surface. The 2D model is established and meshed: the triangular mesh is divided freely, the maximum element size is 37.2 m, the minimum element size is 0.139 m, the curvature factor is 0.25, the maximum element growth rate is 1.2, and the analyzing degree in the narrow zone is 1.

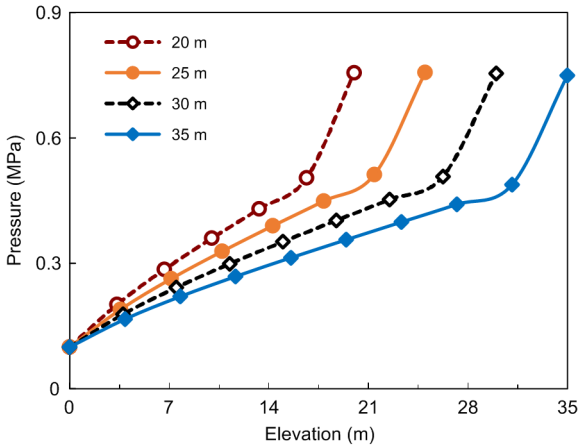

Fig. 13 Pore pressures at the elevation of 0–35 m for different vertical distances (the horizontal plane at the top of the caverns is taken as the zero datum)

Based on the fluid-solid coupling theory, the water-seal of UOSC was evaluated. When the WCP was less than 50 kPa, the water-seal requirements were not met. When the WCP was greater than 100 kPa, the patterns of change in pore pressure around the caverns were similar and tended to be stable (Li et al., 2014). Fig. 14a shows the initial pore pressure distribution, which was not uniform horizontally. The calculated pore pressure distributions

Table 8 Specific values of the pore pressure in Fig. 13 for different vertical distances

35 m		30 m		25 m		20 m	
Elevation (m)	Pressure (MPa)	Elevation (m)	Pressure (MPa)	Elevation (m)	Pressure (MPa)	Elevation (m)	Pressure (MPa)
0.0	0.10	0.0	0.10	0.0	0.10	0.0	0.10
3.9	0.17	3.8	0.18	3.6	0.19	3.3	0.20
7.8	0.22	7.5	0.24	7.1	0.26	6.7	0.29
11.7	0.27	11.3	0.30	10.7	0.33	10.0	0.36
15.6	0.31	15.0	0.35	14.3	0.39	13.3	0.43
19.4	0.36	18.8	0.40	17.9	0.45	16.7	0.51
23.3	0.40	22.5	0.45	21.4	0.51	20.0	0.76
27.2	0.44	26.3	0.51	25.0	0.76	–	–
31.1	0.49	30.0	0.75	–	–	–	–
35.0	0.75	–	–	–	–	–	–

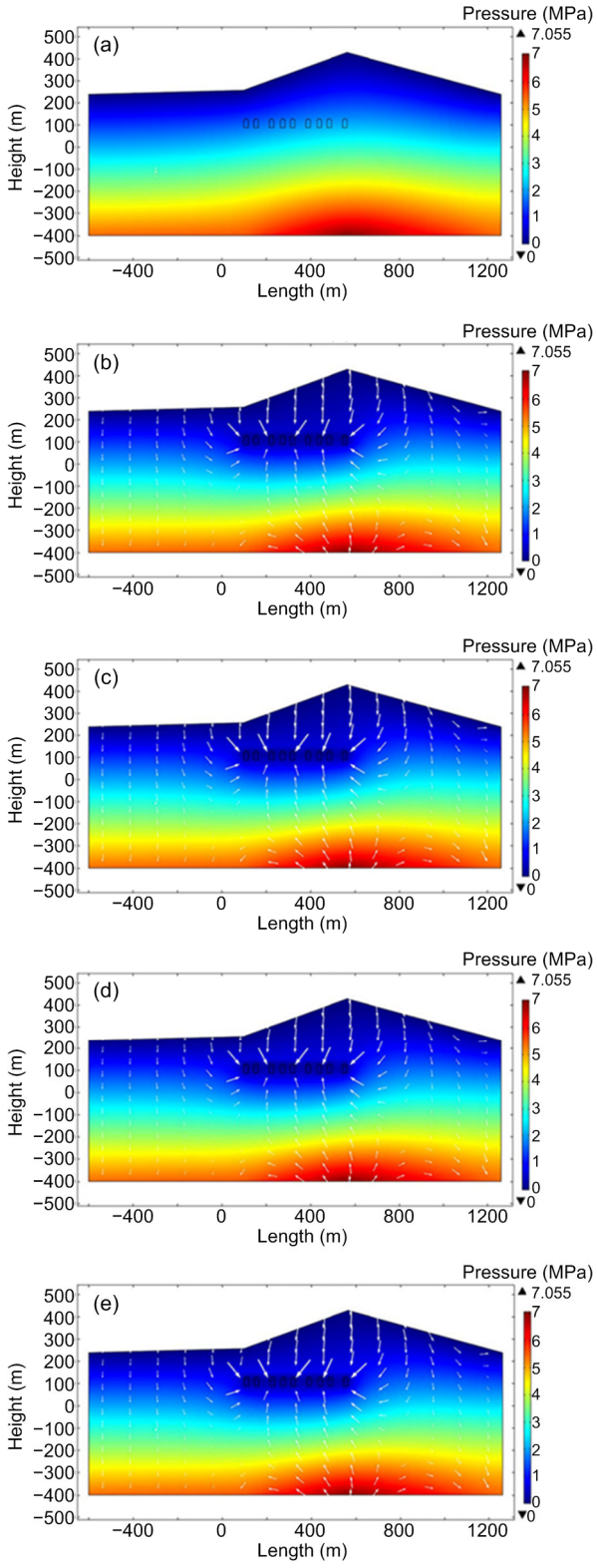

Fig. 14 Pore pressure distributions and fluid velocity vector distributions: (a) initial pore pressure distribution; (b) WCP=60 kPa; (c) WCP=70 kPa; (d) WCP=80 kPa; (e) WCP=90 kPa

and fluid velocity vector distributions under four conditions of WCP are shown in Figs. 14b–14e.

The WCP in this part of the study was tested at 60 kPa, 70 kPa, 80 kPa, and 90 kPa. Fig. 15 shows the pore pressures at the elevation of 0–25 m under different WCPs. Table 9 shows the specific values of the pore pressures shown in Fig. 15. With the increase of WCP, the pressure above the caverns clearly increased. The pressures in the simulation at an elevation of 20 m were 0.45 MPa, 0.52 MPa, 0.59 MPa, and 0.66 MPa (for tested WCPs of 60–90 kPa, respectively). A WCP of 60 kPa cannot meet the water-seal requirements.

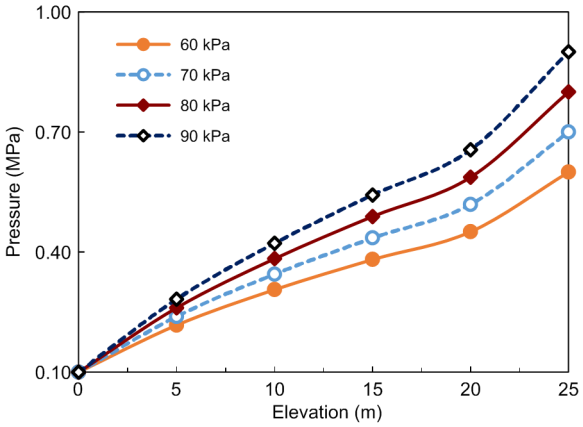

Fig. 15 Pore pressures at the elevation of 0–25 m under different WCPs

Table 9 Specific values of the pore pressures in Fig. 15

Elevation (m)	Pore pressure (MPa)			
	WCP= 60 kPa	WCP= 70 kPa	WCP= 80 kPa	WCP= 90 kPa
0	0.10	0.10	0.10	0.10
5	0.22	0.24	0.26	0.28
10	0.31	0.34	0.38	0.42
15	0.38	0.44	0.49	0.54
20	0.45	0.52	0.59	0.66
25	0.60	0.70	0.80	0.90

The pressures at elevations of 0 m, 10 m, and 20 m (Fig. 16) under four different WCPs were selected for comparative analysis, and the results are shown in Fig. 17. The distributions of pore pressures at elevations of 0 m, 10 m, and 20 m were irregular. The variation in horizontal pressure was more irregular close to the top of the caverns and more stable

away from the caverns. Since the elevation of 20 m is close to the WCHs, the difference in horizontal pore pressure was small. As the WCP is positively correlated with the water inflow into the cavern, it is finite (Li et al., 2009; Xu et al., 2018). The pressure difference between elevations of 0 m and 20 m increased with increasing WCP, which may have caused an increase in water inflow. Taking the pressure at a model body width of 100 m as an example, the pressure difference between elevations of 20 m and 0 m was approximately 0.43 MPa when the WCP was 90 kPa. However, when the WCP was 70 kPa, the pressure difference between the two elevations was approximately 0.25 MPa. Excessive WCP will cause a surge in pore pressure above the caverns. To simultaneously ensure water sealing and minimize water inflow, 70 kPa is a reasonable target for optimal WCP.

Finally, six sections were selected (Fig. 18a) to explore the pore pressure distribution between caverns in an operation period when the WCP was 70 kPa. The distance between the No. 5 and No. 6 caverns is the largest, and the pressure difference between section 1 and section 3 was small, which indicates that the longitudinal pressure distribution between two adjacent caverns increases with the distance between the caverns. The pressure curves of sections 4, 5, and

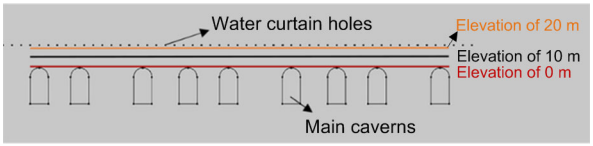

Fig. 16 Study area for Fig. 17

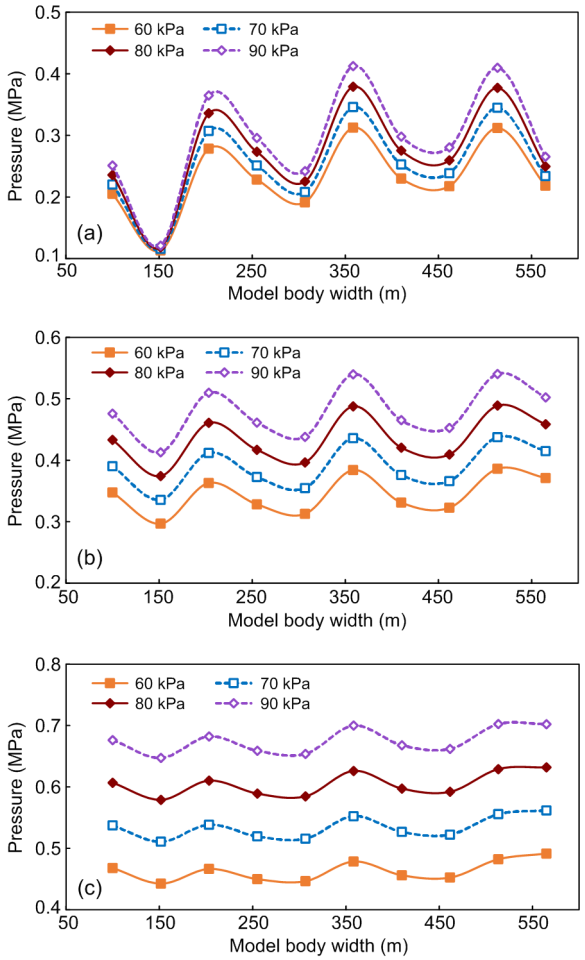

Fig. 17 Pore pressures in the study area at elevations of 0 m (a), 10 m (b), and 20 m (c) (the horizontal plane at the top of the caverns is taken as the zero datum)

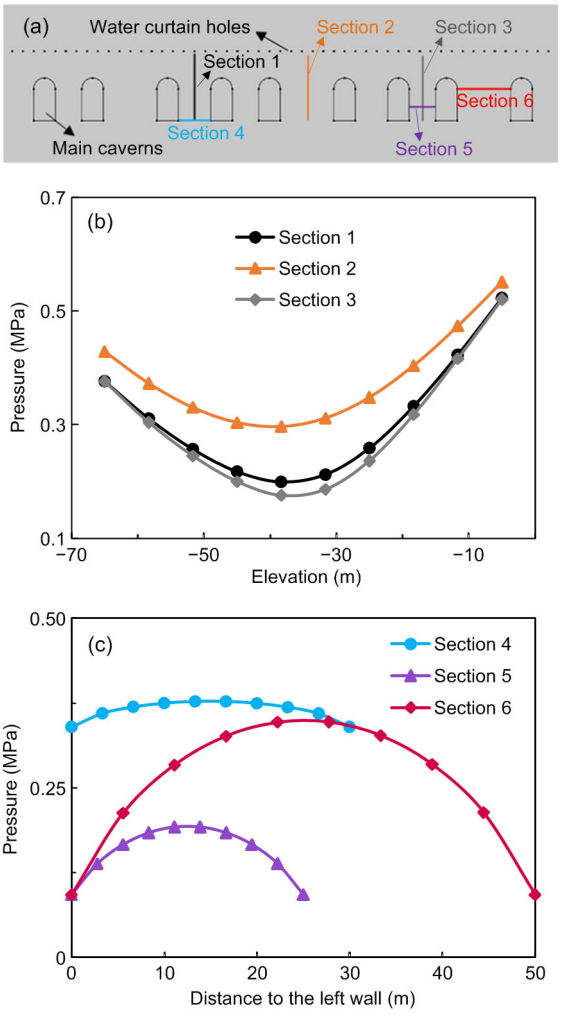

Fig. 18 Pore pressures in the study area: (a) section locations in the study area; (b) vertical sections 1–3; (c) horizontal sections 4–6 (the horizontal plane of the WCH is taken as the zero datum)

6 are approximately symmetrical and have parabolic shapes, which indicates that the pore pressure decreased toward the cavern sidewalls, and that the maximum pore pressure was reached halfway between the two caverns.

6 Discussion

For numerical simulations of UOSCs, a discrete element method (DEM) model can be used. A discrete fracture network (DFN) model was selected to consider the influence of different fracture locations, lengths, and directions on the research results (Wang et al., 2018). The spherical discontinuous deformation analysis (SDDA) method is a recently developed DEM with high calculation speed (Wang et al., 2017). The FEM/DEM model (Wu et al., 2018) combines the advantages of both methods and divides the study body into a porous medium and a fissured medium to incorporate the influence of joint fissures and other geological discontinuities, considering the rock mass as a porous medium rather than a continuous medium.

The design of WCS is complicated by the diversity of its key parameters. This study uses the concept of control variables when dealing with three-factor combination problems, which may lead to the neglect of many other preferred combinations. In the future, a more reasonable design scheme of WCSs will be proposed using an orthogonal experiment.

There are two approximately east-west trending faults that crosscut the caverns at the project location. The faults have a significant impact on the pore pressure around many caverns (particularly No. 1, No. 4, and No. 9 caverns), and the pore pressure around the faults decreases significantly. The influence of faults has not been accounted for in this numerical simulation. The next step in this work will be to further simulate the fault-induced changes in permeability around the surrounding rock and considering their impact on the project and the corresponding mitigation measures. Further, because the numerical simulation used in this study is a simplified 2D model, the influences of complex topography, including geological discontinuities such as joints, construction tunnels, and water curtain tunnel excavation on the project were also not fully accounted for.

7 Conclusions

In this paper, three key parameter design schemes for the WCSs for Huangdao UOSCs are given. The interaction between the surrounding rock, underground water, and liquid oil were considered in a numerical simulation, and it is suggested that the optimal WCH spacing for these UOSCs is 10 m. The water-seal effect is shown to be ineffective when the WCH spacing is larger than 10 m. The water-seal effect enhances with the decreasing of WCH spacing (i.e. smaller than 10 m); however, the enhancement is not effective when considering the economic cost (construction, operation, and drainage costs). Pore pressure decreases rapidly in the range of 5 m around a WCH and decreases slowly outside this range. The long-term stability of the surrounding rock in this range was also closely scrutinized. When the vertical distance between the WCHs and the main cavern is 30 or 35 m, the water-seal is ineffective. A reasonable optimal vertical distance is 25 m. Thus, the vertical influence range of the WCS is currently 25 m. The pore pressure around the main cavern is significantly different due to topographic factors. The vertical pressure distribution between two adjacent caverns increases with increased spacing. When the WCP is 60 kPa, the vertical hydraulic gradient is less than 1. Excessive WCP will cause a sharp increase of pore pressure above the caverns, and the water inflow will also increase. Therefore, 70 kPa is an optimal WCP. For a greater WCP, an increase in water inflow is inevitable.

Contributors

Yi-guo XUE: supervision, conceptualization, methodology. Ze-xu NING: data curation, writing-original draft, software. Dao-hong QIU: methodology, conceptualization. Mao-xin SU: conceptualization, supervision. Zhi-qiang LI: writing-review and editing. Fan-meng KONG and Guang-kun LI: data curation. Peng WANG: final version.

Conflict of interest

Yi-guo XUE, Ze-xu NING, Dao-hong QIU, Mao-xin SU, Zhi-qiang LI, Fan-meng KONG, Guang-kun LI, and Peng WANG declare that they have no conflict of interest.

References

Åberg B, 1978. Prevention of gas leakage from unlined reservoirs in rock. Proceedings of the 1st International Symposium on Storage in Excavated Rock Caverns,

p.399-413.
https://doi.org/10.1016/B978-1-4832-8406-4.50074-9

Aliyu MM, Shang J, Murphy W, et al., 2019. Assessing the uniaxial compressive strength of extremely hard cryptocrystalline flint. *International Journal of Rock Mechanics and Mining Sciences*, 113:310-321.
https://doi.org/10.1016/j.ijrmms.2018.12.002

Chen YM, Xu XB, Zhan LT, 2012. Analysis of solid-liquid-gas interactions in landfilled municipal solid waste by a bio-hydro-mechanical coupled model. *Science China Technological Sciences*, 55(1):81-89.
https://doi.org/10.1007/s11431-011-4667-7

Cornet FH, 2016. Seismic and aseismic motions generated by fluid injections. *Geomechanics for Energy and the Environment*, 5:42-54.
https://doi.org/10.1016/j.gete.2015.12.003

Ehlers W, 2018. Effective stresses in multiphasic porous media: a thermodynamic investigation of a fully non-linear model with compressible and incompressible constituents. *Geomechanics for Energy and the Environment*, 15:35-46.
https://doi.org/10.1016/j.gete.2017.11.004

Hou GX, Shu SZ, 2016. A numerical approach to solve 3D geotechnical problems with 2D codes. Proceedings of the 4th Geo-China International Conference, p.160-166.
https://doi.org/10.1061/9780784480007

Kjørholt H, Broch E, 1992. The water curtain—a successful means of preventing gas leakage from high-pressure, unlined rock caverns. *Tunnelling and Underground Space Technology*, 7(2):127-132.
https://doi.org/10.1016/0886-7798(92)90042-G

Kong F, Shang J, 2018. A validation study for the estimation of uniaxial compressive strength based on index tests. *Rock Mechanics and Rock Engineering*, 51(7):2289-2297.
https://doi.org/10.1007/s00603-018-1462-9

Lee CI, Song JJ, 2003. Rock engineering in underground energy storage in Korea. *Tunnelling and Underground Space Technology*, 18(5):467-483.
https://doi.org/10.1016/S0886-7798(03)00046-4

Levinson G, Ajling G, Nord G, 2004. Design and construction of the Ningbo underground LPG storage project in China. *Tunnelling and Underground Space Technology*, 19(4-5):374-375.
https://doi.org/10.1016/j.tust.2004.02.006

Li SC, Ping Y, Wang ZC, et al., 2012. Assessments of containment and stability of underground crude oil storage caverns based on fluid-solid coupling theory for discrete medium. *Chinese Journal of Rock Mechanics and Engineering*, 31(11):2161-2170 (in Chinese).
https://doi.org/10.3969/j.issn.1000-6915.2012.11.003

Li SC, Wang ZC, Ping Y, et al., 2014. Discrete element analysis of hydro-mechanical behavior of a pilot underground crude oil storage facility in granite in China. *Tunnelling and Underground Space Technology*, 40:75-84.
https://doi.org/10.1016/j.tust.2013.09.010

Li Y, Chen YF, Zhang GJ, et al., 2017. A numerical procedure for modeling the seepage field of water-sealed underground oil and gas storage caverns. *Tunnelling and Underground Space Technology*, 66:56-63.
https://doi.org/10.1016/j.tust.2017.04.002

Li ZK, Wang KZ, Wang AM, et al., 2009. Experimental study of water curtain performance for gas storage in an underground cavern. *Journal of Rock Mechanics and Geotechnical Engineering*, 1(1):89-96.
https://doi.org/10.3724/SP.J.1235.2009.00089

Li ZQ, Xue YG, Qiu DH, et al., 2017. AHP-ideal point model for large underground petroleum storage site selection: an engineering application. *Sustainability*, 9(12):2343.
https://doi.org/10.3390/su9122343

Li ZQ, Xue YG, Li SC, et al., 2019. An analytical model for surrounding rock classification during underground water-sealed caverns construction: a case study from eastern China. *Environmental Earth Sciences*, 78(20):602.
https://doi.org/10.1007/s12665-019-8606-4

Li ZQ, Xue YG, Liang JY, et al., 2020. Performance assessment of the water curtain system: a monitoring system in an underground water-sealed oil reservoir in China. *Bulletin of Engineering Geology and the Environment*, 79(7):3635-3648.
https://doi.org/10.1007/s10064-020-01792-0

Liu RC, Jiang YJ, Li B, et al., 2015. A fractal model for characterizing fluid flow in fractured rock masses based on randomly distributed rock fracture networks. *Computers and Geotechnics*, 65:45-55.
https://doi.org/10.1016/j.compgeo.2014.11.004

Ma XD, Rudnicki JW, Haimson BC, 2017. Failure characteristics of two porous sandstones subjected to true triaxial stresses: applied through a novel loading path. *Journal of Geophysical Research: Solid Earth*, 122(4):2525-2540.
https://doi.org/10.1002/2016JB013637

Ravandi EG, Rahmannejad R, Karimi-Nasab S, et al., 2018. Water curtain system pre-design for crude oil storage URCs: a numerical modeling and genetic programming approach. *Geotechnical and Geological Engineering*, 36(2):813-826.
https://doi.org/10.1007/s10706-017-0355-0

Rouabhi A, Hévin G, Soubeyran A, et al., 2017. A multiphase multicomponent modeling approach of underground salt cavern storage. *Geomechanics for Energy and the Environment*, 12:21-35.
https://doi.org/10.1016/j.gete.2017.08.002

Shang J, Hencher SR, West LJ, 2016. Tensile strength of geological discontinuities including incipient bedding, rock joints and mineral veins. *Rock Mechanics and Rock Engineering*, 49(11):4213-4225.
https://doi.org/10.1007/s00603-016-1041-x

Shang J, Hencher SR, West LJ, et al., 2017. Forensic excavation of rock masses: a technique to investigate discontinuity persistence. *Rock Mechanics and Rock Engineering*, 50(11):2911-2928.
https://doi.org/10.1007/s00603-017-1290-3

Shang J, West LJ, Hencher SR, et al., 2018. Tensile strength of large-scale incipient rock joints: a laboratory investigation.

Acta Geotechnica, 13(4):869-886.
https://doi.org/10.1007/s11440-017-0620-7

Shi L, Zhang B, Wang L, et al., 2018. Functional efficiency assessment of the water curtain system in an underground water-sealed oil storage cavern based on time-series monitoring data. *Engineering Geology*, 239:79-95.
https://doi.org/10.1016/j.enggeo.2018.03.015

Tang ZC, Jiao YY, Wong LNY, et al., 2016. Choosing appropriate parameters for developing empirical shear strength criterion of rock joint: review and new insights. *Rock Mechanics and Rock Engineering*, 49(11):4479-4490.
https://doi.org/10.1007/s00603-016-1014-0

Wang L, Jiao YY, Huang GH, et al., 2017. Improvement of contact calculation in spherical discontinuous deformation analysis. *Science China Technological Sciences*, 60(5):765-771.
https://doi.org/10.1007/s11431-016-0203-6

Wang ZC, Li SC, Qiao LP, 2015. Design and test aspects of a water curtain system for underground oil storage caverns in China. *Tunnelling and Underground Space Technology*, 48:20-34.
https://doi.org/10.1016/j.tust.2015.01.009

Wang ZC, Li W, Qiao LP, et al., 2018. Hydraulic properties of fractured rock mass with correlated fracture length and aperture in both radial and unidirectional flow configurations. *Computers and Geotechnics*, 104:167-184.
https://doi.org/10.1016/j.compgeo.2018.08.017

Wu N, Zhang C, Maimaitiyusupu S, et al., 2019. Investigation on properties of rock joint in compression dynamic test. *KSCE Journal of Civil Engineering*, 23(9):3854-3863.
https://doi.org/10.1007/s12205-019-1779-2

Wu ZJ, Ma LL, Fan LF, 2018. Investigation of the characteristics of rock fracture process zone using coupled FEM/DEM method. *Engineering Fracture Mechanics*, 200:355-374.
https://doi.org/10.1016/j.engfracmech.2018.08.015

Xu ZH, Gao B, Li SC, et al., 2018. A groundwater seal evaluation method based on water inflow for underground oil storage caverns. *Tunnelling and Underground Space Technology*, 82:265-277.
https://doi.org/10.1016/j.tust.2018.08.030

Xue YG, Li SC, Qiu DH, et al., 2015. A new evaluation method for site selection of large underground water-sealed petroleum storage depots. *Science China Technological Sciences*, 58(6):967-978.
https://doi.org/10.1007/s11431-015-5825-0

Yan L, Meng QX, Xu WY, et al., 2017. A numerical method for analyzing the permeability of heterogeneous geomaterials based on digital image processing. *Journal of Zhejiang University-SCIENCE A (Applied Physics & Engineering)*, 18(2):124-137.
https://doi.org/10.1631/jzus.A1500335

Yang TH, Jia P, Shi WH, et al., 2014. Seepage-stress coupled analysis on anisotropic characteristics of the fractured rock mass around roadway. *Tunnelling and Underground Space Technology*, 43:11-19.
https://doi.org/10.1016/j.tust.2014.03.005

Ye B, Cheng ZR, Ye WM, et al., 2019. An analytical solution for analyzing the sealing-efficiency of compressed air energy storage caverns. *KSCE Journal of Civil Engineering*, 23(5):2025-2035.
https://doi.org/10.1007/s12205-019-0260-6